Prepared for submission to JHEP

Light Dark Matter eXperiment (LDMX): Conceptual Design Report

an author[a]

[a] *an institution*

Abstract: this is good stuf

Contents

---

1 Overview and Executive Summary (Editors: Philip Schuster, Gordan Krnjaic)

2 Science Goals (Editors: Philip Schuster, Gordan Krnjaic)

2.1 Dark Matter

- sub-GeV dark matter - summary of production kinematics

2.2 Fundamental Forces

- hidden photons, scalars...etc - summary of production kinematics

2.3 Nuclear Physics

- rare photo-nuclear reactions

3 Detector Concept

Basic Considerations and Overview

- Signal characteristics
- Possible backgrounds
- Achieving high luminosity
- Explain why we want a tagger tracker, moderate 0.1 X0 target, recoil tracker, high granularity calorimeter, hadronic veto
- Summarize the overall layout of the experiment

3.1 Beamline (Editors: Tim Nelson, Omar Moreno)

The LDMX beamline is relatively simple, consisting only of an analyzing magnet and a vacuum chamber into which the tagging and recoil trackers are installed. The analyzing magnet is a common 18D36 dipole magnet with a 12-inch vertical gap and operated at a central field of 1.5 T. A stainless-steel vacuum chamber with 1/2" walls fits just inside the magnet bore supporting the tracking detectors and their readout electronics. The upstream end of the vacuum chamber is closed by a plate with a 6" conflat flange for connection to the upstream beampipe and the downstream end is closed by a titanium vacuum window in front of the ECal face which sits 20 cm downstream of the target at roughly the same z position as the outer face of the magnet coils. The magnet is rotated by approximately 100 mrad about the vertical axis with respect to the upstream beamline so that the incoming 4 GeV beam follows the desired trajectory to the target, with the incoming beam arriving at normal incidence to, and centered on, the target. Although the specific dimensions differ, this arrangement (aside from the vacuum window) is very similar to the magnet and vacuum chamber employed by the HPS experiment at JLab. As with HPS, additional vacuum boxes at the upstream and/or downstream ends will be appended to the vacuum chamber to accommodate feedthroughs for power, readout and cooling.

3.2 Tagging Tracker (Editors: Tim Nelson, Omar Moreno)

3.3 Target (Editors: Tim Nelson, Omar Moreno)

3.4 Recoil Tracker (Editors: Tim Nelson, Omar Moreno)

3.5 Forward Electromagnetic Calorimeter (Editors: Joe Incandela)

3.6 Hadronic Veto System (Editors: Jeremy Mans, Nhan Tran, Andrew Whitbeck)

It is also important to extend the calorimeter to veto neutral hadrons being produced in photo-nuclear reactions. As exclusive reactions of this type are rare, the rates and radiation

doses will be much lower as the design for the HG calorimeter is designed to fully contain the electromagnetic showers. This removes the requirement for silicon in the hadronic calorimeter section. A scintillator-based sampling calorimeter is a natural solution in this situation. The goal of the hadronic veto system is to identify neutral hadrons in the energy range from above approximately 100 MeV to several GeV with high efficiency. This requires a hadronic calorimeter with at least 5 nuclear interactions of depth in order to fully contain the most energetic of neutrons with greater than 99% probability. Simultaneously, in order to detect lower energy neutrons, absorbing layers cannot be too thick such that neutrons of hundreds of MeV are captured in the absorbers. Therefore, a steel-scintillator (polystyrene) calorimeter of approximately 15 layers and totaling 5 nuclear interaction lengths is proposed. Each layer is structured as 50 mm of Steel, 2 mm air gap, 6 mm of scintillator, and 2 mm of air gap where the air gaps are left for detector services. The transverse size of each layer is 1 x 1 m to cover the solid angle of the signal acceptance. Transverse granularity of the system is not required due to the lower rates expected in the hadronic system and in order to maintain high efficiency for neutral hadron detection. An illustration of the hadronic veto system is given in Fig. 1.

Figure 1. Placeholder... Drawing of HCAL, is it needed? Could be integrated into a full detector rendering

Fast readout is also required of the hadronic calorimeter system in order to coincide with electromagnetic calorimeter information. Readout will be based on the CMS Phase 1 upgrade HCAL system which has fast readout capabilities intrinsically at frequencies of 40 MHz and would be sufficient for the DASEL beam structure. Scintillating light is read out by wavelength shifting fibers with silicon photomultipliers (SiPMs) as the photodetectors. SiPM technology is chosen due to high gain and low noise capabilities. Each layer is read out by N wavelength shifting fibers and the light is optically summed into M photodetectors In addition to the SiPMs, readout modules (48/64 channels per) and charge integration electronics designed for the CMS detector can be re-purposed for the LDMX experiment with minimal changes and takes advantage of experience of CMS collaborators on LDMX. The timescale for commissioning of the readout electrons in CMS are 2017/2018 and thus are appropriate for the LDMX timeline.

3.7 Wide-Angle Calorimeter ??

3.8 Trigger System (Editors: Jeremy Mans, Nhan Tran, Andrew Whitbeck)

The LDMX trigger system is designed to reduce the typical beam particle arrival rate of $\approx$ 40 MHz to a rate of O(1 kHz) for storage and analysis. The selection is performed by a combination of dedicated hardware and software running on general-purpose computers.

Figure 2. Drawing of the trigger fiber hodoscope

The first stage trigger is implemented in hardware and allows the selection of both candidate events for dark matter production and important samples for calibration and detector performance monitoring. The overall trigger management is provided by a trigger manager board, which receives inputs from the various triggering subsystems including the silicon calorimeter and the scintillator calorimeter. The latency requirements on the trigger calculation latency are set by the tracker readout ASIC to 2us.

The primary physics trigger is based on the silicon calorimeter and is designed to select events with energy deposition significantly lower than the full beam energy. The silicon calorimeter ASIC calculates the total energy in 2x2 fundamental cells for every 40 MHz pseudo-bucket. The energy information is transferred by digital data link to the peripherary of the calorimeter, where sums can be made over larger regions and transferred by optical link to the trigger electronics. The total energy is then used to select the events.

The use of a calorimeter trigger requirement of energy below a threshold also requires a beam-presence measurement to avoid very high trigger rates during crossings where there is no beam electron present. The trigger fiber hodoscope is designed to serve this purpose. The hodoscope is constructed of an array of 1 mm-diameter scintillating fibers, which are mounted immediately upstream of the tungsten target. [more details on the mechanics, including orientation of the fibers]

The fibers from the hodoscope are brought to an optical vacuum feedthrough and a clear fiber ribbon is connected on the outside of feedthrough to carry the light signals to the readout electronics. Based on studies by the LHCb collaboration[**?**], scaled to the diameter of fibers in use for the hodoscope, we expect a typical signal of [] photons to be produced in the hodoscope by a beam electron after a total absorbed radiation dose of XXX Gray. We expect to able to bring at least [50%] of these photons to the readout SiPMs.

The same electronics design is used for readout of the hodoscope and the scintillator calorimeter. This readout is based on SiPMs and the housing is designed to allow operation of the SiPMs at reduced temperatures (below 5°C) to reduce the thermally-induced single-photon noise. The typical photodetector efficiency of these SiPMs is [30%][**?**], providing a typical signal of [] PEs in the electronics. The readout electronics will continuously digitize the SiPM signal, providing an integrated charge as well as time-of-arrival measurement for the pulse with an LSB of 500 ps. Both amplitude and timing information can be provided to the trigger, allowing the correction of the calorimeter amplitude for timewalk effects already at trigger level.

3.9 DAQ (Editors: Jeremy Mans, Nhan Tran, Andrew Whitbeck)

4 Physics and Detector Simulation

Simulations Overview (Editors: Natalia Toro, Jeremy McCormick)

This section describes the methods used to simulate signal and background physics reactions and the responses of various detectors to these reactions. For historical reasons, two separate simulation frameworks have been used: the "tracker simulation" implemented in SLIC comprises a full simulation of the tagger tracker and recoil tracker, with ECAL material included but not its detector response. Likewise, the "calorimeter simulation" implemented directly in Geant4 comprises a full simulation of the ECAL and HCAL, with recoil tracker material included upstream. In both cases, the target material and magnetic field map are also included. Please check for accuracy These two simulations are described in more detail in §**??**–**??**.

While the primary simulation engine is Geant4 [**?**], the signal reaction (Dark Matter pair production) is modelled using an external generator based on MadGraph/MadEvent4 [**?**]. This generator, its validation, and the interface with Geant4 are described in §**??**. All background processes are modelled directly in Geant4, with modifications and biasing for photonuclear processes as discussed in §**??**.

4.1 Simulation of the Tagger and Recoil Trackers (Editors: Omar Moreno, Jeremy McCormick)

The simulation of the passage of both charged and neutral particles through both the tagger and recoil trackers uses a software package based on SLAC's org.lcsim infrastructure which wraps Geant4. The simulation creates realistic charge depositions in the silicon layers, simulates the APV25 readout chip amplifier chain as well as the 24 ns sampling of the signal, creates clusters and performs track finding. The performance studies assumed that the tagger (recoil) tracker is within a uniform dipole field of strength -1.5 T (-.75 T), while all acceptance studies use the full field map. A rendering of the tagger and recoil tracker as used in the simulation is shown on Figure **??**.

4.1.1 Readout simulation

4.1.2 Hit Reconstruction

The six samples emerging from each channel are fit using the following 3-pole function

$$f(t) = A\frac{\tau_1^2}{(\tau_1-\tau_2)^3}\left(e^{-\frac{t-t_0}{\tau_1}} - \sum_{k=0}^{2}\left(\frac{\tau_1-\tau_2}{\tau_1\tau_2}(t-t_0)\right)^k \frac{e^{-\frac{t-t_0}{\tau_2}}}{k!}\right) \tag{4.1}$$

where τ_1 and τ_2 represent the fall and rise time of the shaper signal respectively. The amplitude, A, and the time of the hit, t_0, are then determined from the fit.

Hits on neighboring strips are clustered using a nearest neighbor algorithm as follows:

- A list of seeds is created from all raw hits that have an amplitude, S, $> 4 \times \sigma_{\text{Noise}}$

- Recursively add neighboring strips that have $S > 3 \times \sigma_{\text{Noise}}$ until a strip with $S < 3 \times \sigma_{\text{Noise}}$ is found.
- Require that neighboring hits have a t_0 that is within 8 ns of the seed hit.
- Repeat the first two steps until seed strips are no longer found.
- Require that a cluster has an amplitude $> 4 \times \sigma_{\text{Noise}}$.

After hits on a sensor have been clustered, the cluster time is computed as the amplitude-weighted average of the t_0 times from the hits that compose it. All clusters in adjacent pairs of layers are combined to create 3D hits.

4.1.3 Track Reconstruction

The track finding and fitting algorithm proceeds in steps following a specific "tracking strategy". The strategies outline which layers are used, the minimum number of hits required to form a track and kinematic constraints. The algorithm proceeds as follows:

- All possible combinations of hits are formed from the seed layers and and a helix fit is performed. Only those seeds which satisfy a χ^2 requirement are kept.
- Once all seeds have been found, hits from a specified "confirm" layer are added to the seeds and a helix fit is performed once again. Those fits which do satisfy a χ^2 cut are eliminated.
- Finally, tracks are "extended" by hits from the rest of the layers. After the addition of a hit, a helix fit is performed. If the track fails the χ^2 constraint, the hit is discarded. This procedure is repeated until all hits in a layer have been added to all seeds, however, it is possible for all hits in a layer to be discarded.
- All track candidates are merged in order to form a set of unique tracks. Tracks are allowed to share at most one hit. If a pair of tracks shares more than a single hit, the track with the best chi^2 is chosen.

Need to talk about what strategy and cuts are being used.

4.2 Simulation of the Calorimetry Systems (Editors: Owen Colegrove, Joe Incandela)

A common simulation framework is utilized for the electromagnetic and hadronic calorimeter systems based solely on `GEANT4`. In addition to a full implementation of the sampling layers for both calorimeters, the target, recoil tracker and magnetic field are also included.

4.2.1 Digitization of Forward Electromagnetic Calorimeter

add stuff here, make it common with trigger description?

4.2.2 Digitiztaion of the Hadronic Veto System (Editors: Nhan Tran, Andrew Whitbeck)

After full `GEANT4` simulation, we simulate the digitization of the particle-level interactions in our detector to understand how well we can reconstruct events in the hadronic calorimeter. Given the particle-level energy deposition per layer, we can convert that into the number of minimum ionizing particles (MIP) that we expect in that layer. The translation comes by first estimating the typical energies deposited in a calorimeter model for a MIP. This can be seen in Fig. 3 where a distribution of energies deposited in a given layer is shown for a single MIP muon.

By translating the energy deposited into a single layer, we can compute how many MIPs we expect in a given layer in a given event. From CMS testbeam studies [], it is computed that 1 MIP corresponds to about 13.5 photo-electrons measured in the SiPM. We then set the threshold for a layer becoming vetoed in our detector simulation based on number of photo-electrons measured in the SiPM That threshold is set at 9 photo-electrons which is $> 4\sigma$ above the typical noise in SiPMs which is typically 2 photo-electrons.

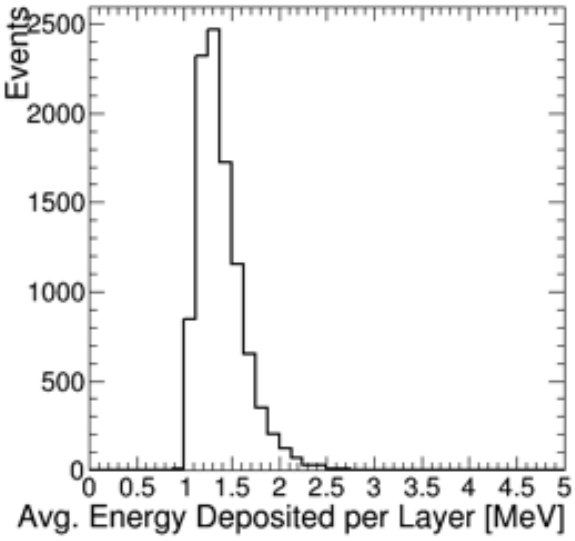

Figure 3. Distribution of energies deposited in scintillator from muon to characterize MIP behavior in plastic scintillator

4.3 External Physics Generator for Signal Reaction (Dark Matter Production) (Editor: Natalia Toro)

While background processes are modelled entirely in the Geant4 framework, the new physics of Dark Matter production is modelled using an external event generator based on MadGraph/MadEvent4 [**?**]. Here we describe this generator, its validation, and the interface with Geant4.

MadGraph is an automated tool for calculating the tree-level amplitudes for arbitrary physics processes, which allows users to define Feynman rules for new physics models; MadEvent is a Monte Carlo event generator based on MadGraph. MadGraph/MadEvent4 (MG/ME) was designed for the study of high-energy collider reactions, but minor modifications to the code (introducing non-zero masses for incident particles and for the electron, and an electromagnetic form factor as described in [**?**] for the nucleus) allow for its application to fixed-target processes. These modifications and a new-physics model that introduces a dark photon with arbitrary mass and kinetic mixing ϵ with the photon has been used for the APEX test run [**?**] and HPS experiment [**?**]. For LDMX, we have added light dark matter particles (either fermions or scalars) that couple to the dark photon with an arbitrary interaction strength g_D. This allows us to simulate the signal process of DM particle pair-production via either decay of an on-shell A' or off-shell A' exchange. This report focuses on the on-shell production process, though the kinematics of the two are very similar.

Do we want to say something explicit about the form factors?

Within MG/ME, we generate events for the DM production process $e^- W \to e^- W\,(A' \to \chi\bar{\chi})$ where χ represents the dark matter particle and $\bar{\chi}$ its antiparticle. Events are generated assuming a 4 GeV incident electron and Tungsten nucleus at rest as the initial state. MG/ME computes a Monte Carlo approximation of the inclusive cross-section for this process, and generates a sample of unweighted events in the Les Houches Event (LHE) format [**?**]. The inclusive cross-section computed by MadGraph is stable within 1% and is consistent within $\sim 30\%$ with independent calculation of the cross-section in the Weizsacker-Williams (WW) approximation from [**?**]. The deviations from the WW inclusive cross-section are largest at high and low masses, and compatible with the size of errors expected in the WW approximation.

[IS THSI RIGHT?] To seed Geant4 events from the MG/ME output, we read the four-momentum of the recoiling electron and Tungsten nucleus?? from the LHE file and use these to populate an STDHEP event. The electron and nucleus are assumed to originate from a common vertex, uniformly distributed over the thickness of the target and over a transverse region spanning **CHECK!** ± 1 **cm in the** x **direction and** ± 2 **cm in the** y **direction about the nominal center of the target.**

4.4 Photonuclear Model and Biasing (Editors: Natalia Toro, Omar Moreno)

5 Performance Studies

Baseline luminosity: We want to handle 4×10^{14} electrons on target (EOT) with incoming energy of 4 GeV.

5.1 Signal Characteristics

Please note that we need to optimize the energy selection used below. Starting definition:

Tracking:

- One incoming beam electron with E_{beam} close to 4 GeV and a well measured trajectory.
- Quality cuts (as needed) to reduce any dangerous brem (or photo-nuclear) reactions in the tagger tracker material
- One recoiling electron with $E \lesssim 1.2$ GeV that points back to the incoming beam electron track.
- An activity cut in the recoil tracker to reject photo-nuclear reactions in the target
- An inferred "missing momentum" trajectory and magnitude

Calorimetry:

- One soft recoil shower with $E \lesssim 1.2$ GeV that is consistent with recoil tracker trajectory
- An activity cut in the "missing momentum" region for the ECal
- An explicit veto on energetic (energy range needs to be specified) hadrons in both the ECal and hadron veto system

5.2 Tagging Tracker Performance (Editors: Tim Nelson, Omar Moreno)

The tagging tracker must identify incoming beam-energy electrons with extremely high purity, suppressing the mis-reconstruction of any incoming low-momentum charged particles as beam energy electrons. In particular, any incoming charged particle within the recoil acceptance for signal that is reconstructed as having the beam energy in the tagging tracker is an irreducible background. The design of the tagging tracker makes the likelihood of such errors vanishingly small, with good resolution for both beam energy and off-energy incoming tracks and an exceedingly low rate of mis-reconstruction for tracks within the recoil energy acceptance.

In order for an incoming low momentum particle to fake a beam energy electron in the tagger, a number of conditions must simultaneously be met:

1. The incoming particle must reach the first tagger layer or it will not intersect with any material until it hits the wall of the vacuum chamber.

2. The particle must either scatter in each layer in order to fake a 4 GeV track or create secondaries that generate occupancy which confuses the pattern recognition in the tracker resulting in reconstruction of a fake 4 GeV track.

3. The resulting track must have a trajectory consistent with that of a typical 4 GeV beam electron all the way through the tracker.

4. The resulting track must have an impact point at the target consistent with a reconstructed track within the signal acceptance in the recoil tracker.

Using an analytic model of the tagging tracker that includes the effect of intrinsic resolutions and multiple scattering in the tracker planes, it is evident that each of these requirements places a very heavy penalty on any off-energy component in the beam. First, incoming particles with less than approximately 500 MeV momentum will not hit the first layer of the tagger unless they are significantly off-trajectory as well. Furthermore, even at 500 MeV, a first scatter of more than 10° is needed in order for the incoming particle to appear to be on the correct trajectory. It is clear then that the most challenging scenario is large contamination with incoming charged particles at the top of the momentum range for signal recoils, nominally 1.2 GeV. Such particles have the highest likelihood of reaching the first layer of the tagger tracker without being bent away by the magnetic field and require much smaller scatters and/or track reconstruction errors to result in fake tags. In order for a 1.2 GeV particle to make a trajectory through the tracker consistent with a 4 GeV track, six successive scatters of approximately ten milliradians must occur, each equivalent to approximately 15σ on the multiple scattering distribution. From the tails of the Moliere scattering distribution, the likelihood of each of these scatters is smaller than one per million. Therefore, the much more likely scenario is the generation of secondaries an the material of the tagger tracker followed by misreconstruction of a fake 4 GeV track. Since the resulting 4 GeV track must arrive at the target on the correct trajectory and beam energy electrons arrive normal to the target with a one-sigma error of 250 microradians, there is very little phase space for randomly reconstructed 4 GeV fakes to have the correct trajectory. Finally, any falsely reconstructed 4 GeV track must have a common impact point in the target with a real track of matching momentum in the recoil tracker, which is unlikely for a falsely reconstructed tracks.

In order to more fully test these scenarios, two samples of incident electrons were simulated and reconstructed in the tagger tracker. The first is a sample of XXX 4 GeV electrons on the nominal beam trajectory. The second is a sample of XXX 1.2 GeV electrons on a trajectory that allows them to pass through all seven layers of the tagging tracker. The 4 GeV sample confirms the expected resolutions, as shown in Figures **??**.

These indicate that tight requirements can be made in both the energy and trajectory at the target that rejects off-momentum particles that could be present in the incoming beam and that the tagging tracker identifies a precise impact position that can be used for tracking recoil candidates. The 1.2 GeV sample confirms at the level of 1 part in $10^{?}$ that these tracks cannot be mistaken for 4 GeV tracks, as shown in Figure 6. In order to probe the likelihood

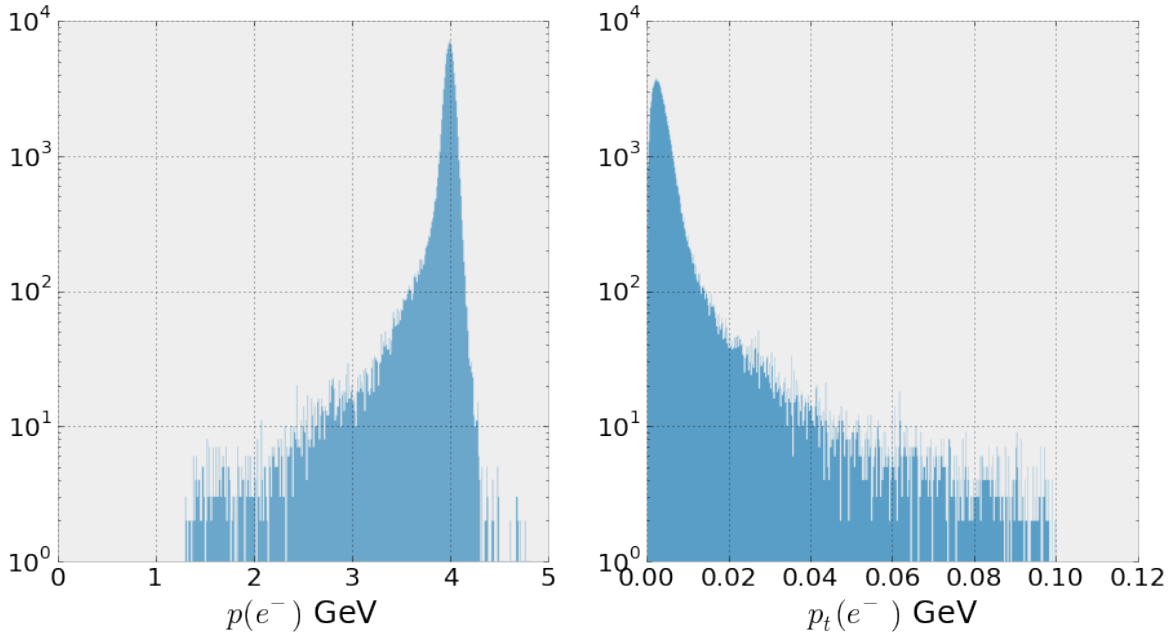

Figure 4. Reconstructed total momentum and momentum transverse to target for a sample of 4 GeV beam electrons.

Figure 5. Reconstructed Tagger track x-y position at the target for a sample of 4 GeV beam electrons.

of reconstructing fake 4 GeV tracks at higher statistics we further introduce random noise hits on all planes of the tracker at rates of 10^{-3}, 10^{-2} and 10^{-1} in all planes of the tracker, where typical noise occupancies in similar HPS modules are roughy 10^{-4}. Figure 7 shows the resulting distribution of reconstructed tracks in energy and p_T at the target. Obviously, such extreme occupancies in the tracker are atypical, and would easily be selected against with negligible impact on signal efficiency. Furthermore, these fake tracks, not being due to an individual low-momentum track, will typically not align with a low-momentum track in the recoil tracker. Although further study will be required to find the beam intensity limits for this tagging tracker design, we can safely conclude that it is more than capable of providing the tagging purity required for the first stage of the LDMX experiment.

5.3 Recoil Tracker Performance, (Editors: Tim Nelson, Omar Moreno)

Needs to be spelled out in more detail...

- Acceptance
- Efficiency
- What kind of activity cuts do we want to apply? Background rejection power? Signal efficiency?

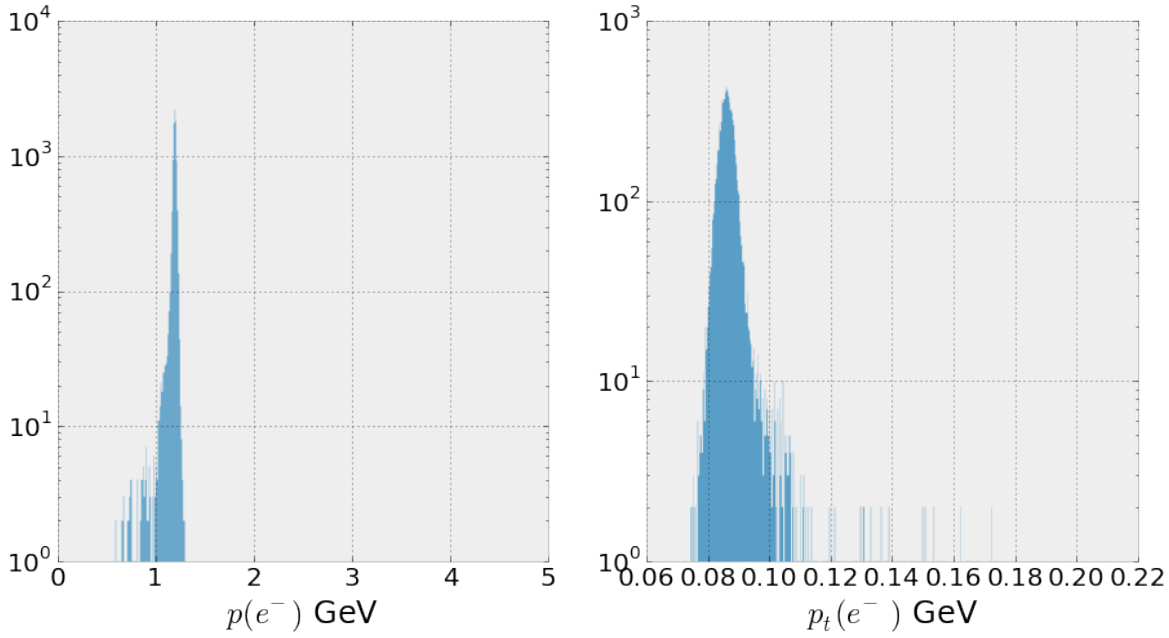

Figure 6. Reconstructed total momentum for a sample of 1.2 GeV beam electrons.

Figure 7. Reconstructed momentum vs. momentum transverse to the target for a sample of 1.2 GeV electrons in the presence of 10^{-3}, 10^{-2} and 10^{-1} random occupancy in all sensors.

5.4 Forward Electromagnetic Calorimeter (Editors: Joe Incandela)

Owen and Joe will discuss this at the July 8 meeting. But Philip's notes include:

- Hermiticity: make sure to include a study of cracks or dead material in the detector simulation. Do we need to worry about this? Why?

Large scale "top down" monte carlo study to demonstrate baseline performance of ECal and to justify more detailed study of specific reactions that dominate the tail of low energy deposition events. We need to quantify everything I'm about the say more carefully. Starting from 4×10^{14} EOT, the baseline tracker selections bring the event sample down to $\sim 4 \times 10^{12}$. So we're dealing with $\sim 4 \times 10^{12}$ events with a soft recoiling electron and a hard, ~ 3 GeV, photon. ECal events that are hadron rich occur about $\sim 10^{-3}$ of the time. So now we're down to $\sim 4 \times 10^{9}$ hadron rich events in the ECal.

- most importantly, we want to understand what dominates the low energy deposition events

- we want to characterize the hadron rich events (because we know they are a potential issue)

- explain veto strategy

- at what point is the energy deposition so low that it's not possible to veto effectively? what are these events types?

Specific "bottom up" studies of photo-nuclear reactions: We know that certain event types could pose a challenge, so let's study them. The numbers shown below are with very loose kinematic selections, so they are upper bounds. They are also for 9 GeV photons, so Philip and Natalia will need to correct them. This is a good starting point for study however:

- $\gamma N \to (\rho, \omega, \phi)N \to \pi^+\pi^- N$ ($\lesssim 10^8$ of this event type).
- $\gamma N \to \mu^+\mu^- N$ ($\lesssim 2 \times 10^7$ of this event type).
- $\gamma p \to \pi^+ n$ ($\lesssim 4 \times 10^5$ with $\sim 4 \times 10^3$ of these having a backscattered π^+).
- $\gamma n \to n\bar{n}n$ ($\lesssim 4 \times 10^5$ of this type).
- $\gamma(p, n) \to K_L K_L + X$ (expect this at the $\sim 10^3$ level, but we need to check this!)

The current plan is to use a particle gun and weight the depth of origination and angle/energy distribution using data. Let Philip and Natalia know when you're ready to do this. *We need to be especially careful to include the regions of phase space where the MIPs are soft or wide/back scattering by recoiling off the nucleons or atoms. This needs a dedicated study, starting with the physics simulations group, P,N,E,G.*

5.5 Hadronic Veto System (Editors: Jeremy Mans, Nhan Tran, Andrew Whitbeck)

The hadronic veto system is designed for detecting rare processes and therefore studies of its performance focus on "bottom up" vetoes of photo-nuclear reactions. If we consider that the rare processes described in Section **??** should produce a low multiplicity of neutrons we perform studies to compute on the efficiency the hadronic veto system of a detecting single neutron. This will give us an idea of the efficiency with which we can veto any type of photo-nuclear reaction based on the hadronic system only.

We benchmark the hadronic veto system by considering neutrons, being generated at the face of the calorimeter, with various:

- energies: 1.3, 1.5, 1.8, 2.0, 2.2, 2.5, 3.5 GeV (total energy)
- number of calorimeter layers: 15, 20, 25
- incident angles: 0, 15, 30 degrees

For each neutron phase space point, we generate 5×10^4 events.

First we study the propagation of neutrons through the HCAL purely via `GEANT` without yet considering the digitization of the scintillation signal, which was described in Section 4.2.2. We define the kinetic energy flux for a given layer as the amount of kinetic energy passing through the front face of a given HCAL layer. In Fig. 8, we show the neutron kinetic energy flux as a function of HCAL layer for 3.5 GeV total energy neutrons produced at an incident angle of 0.0°. We note that the "shower max" for hadronic showers in this system is typically around layers 6/7. By looking at the neutron flux around a kinetic energy of 2.5 GeV as a function of layers, we can estimate the fraction of neutrons which pass directly through the calorimeter without interacting. We can conclude that roughly 100/50000 $\sim$ 0.2% of

neutrons do not interact in the first 15 layers of the system. This number drops to roughly 0.02%(0.002%) for a 20 (25) layer system. This fraction is independent of incident neutron energy.

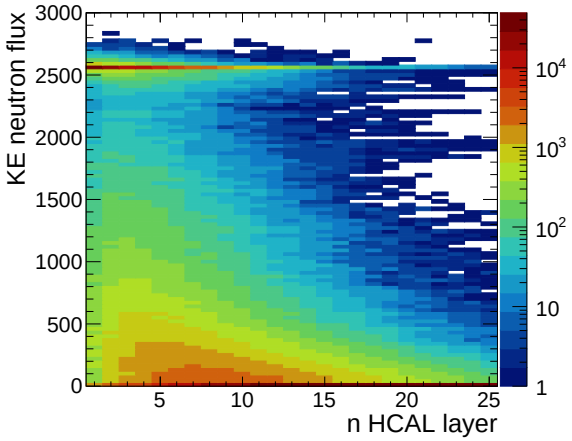

Figure 8. Neutron kinetic energy flux through the HCAL as a function of layer for a 3.5 GeV neutron produced with an incident angle of 0.0° at the front face of the calorimeter.

For neutrons that do interact in the HCAL, we then compute the efficiency of detecting them given a simple digitization process described in Section 4.2.2. As a reminder, we assume that a MIP deposits, on average, 1.4 MeV of energy in the scintillator, which from CMS testbeam studies we estimate translates into 13.5 photo-electrons at the SiPM. Given a typical noise contribution of 2 photo-electrons in SiPMs, we define a MIP signal in a given layer as 8 photo-electrons. Therefore, we define a *MIP layer* as a scintillator layer in the HCAL in which enough energy is deposited to produce at least 8 photo-electrons (Poisson-varied). We define a vetoed neutron event as a neutron which has created ≥ 1 MIP layer. The number of MIP layers is plotted in Fig. 9 for an incident 2.5 GeV total energy neutron assuming a system of 15, 20, or 25 layers; or in other words, counting only MIP layers in the first 15, 20, or 25 HCAL layers (left to right). In Fig. 9, we can count the number of events in the 0 bin of each plot to find the fraction of neutron events which would *not* be vetoed, which we call *mis-vetoed* neutrons. For an incident 2.5 GeV total energy neutron, the fraction of mis-vetoed depends strongly on the number of HCAL layers in the system. This suggests, for higher energy neutrons, that the mis-veto fraction is dominated by neutrons which do not interact in the system and are not contained.

The number of MIP layers is plotted in Fig. 12 for an incident 1.3 GeV total energy neutron assuming a system of 15, 20, or 25 layers (left to right). Here, we note that the mis-veto efficiency is fairly constant as a function of the number of HCAL layers in the system. We conclude that most mis-vetoed neutron events for lower energy neutrons do not deposit enough energy in the scintillator to pass the threshold for a MIP layer or are directly absorbed

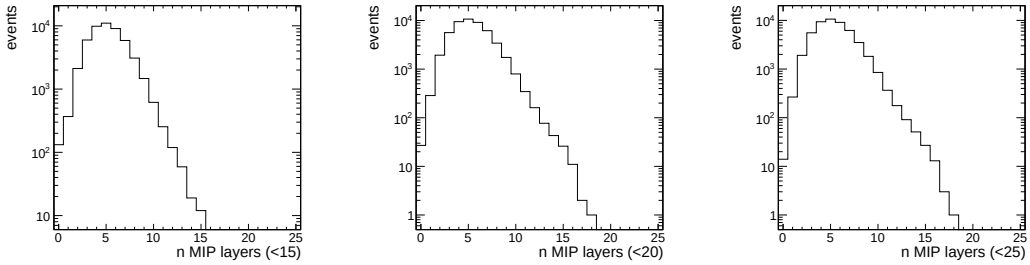

Figure 9. Number of MIP layers for a 2.5 GeV neutron produced with an incident angle of 0.0° at the front face of the calorimeter for a system of 15, 20, or 25 layers (left to right).

into the Steel absorber layer.

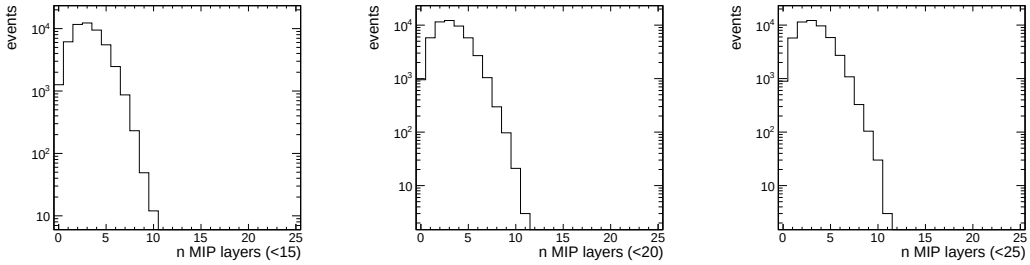

Figure 10. Number of MIP layers for a 2.5 GeV neutron produced with an incident angle of 0.0° at the front face of the calorimeter for a system of 15, 20, or 25 layers (left to right).

Finally we conclude by benchmarking performance as a function of number of layers in the system and incident neutron angle. This is shown in Fig. **??**. Here we show the neutron mis-veto rate as a function of total energy, incident angle. and number of HCAL layers. First we see that the mis-veto rate fall quickly with energy which indicates that we are much more efficient at detecting higher energy neutrons at a mis-veto rate of $10^{-}3$-$10^{-}5$ depending on the number of layers in the system and the incident angle of the neutron. At higher energies, a larger incident angle or more layers reduces the mis-veto rate where in both cases the neutron traverses more material (absorber). This indicates that the main source of mis-vetoed neutrons comes neutrons that do not interact with the HCAL. For lower energies, the mis-veto rate for neutrons is practically independent of incident angle and number of layers and is typically at a value of $10^{-}1$.

In Fig. **??**, we show a more fine-grained mis-veto rate plot with more neutron energies considered.

to add: studies changing absorber thickness and varying MIP layer threshold. Further studies are on-going to better improve performance at lower energies.

From single neutron studies, we conclude that we are able to veto neutrons at an event

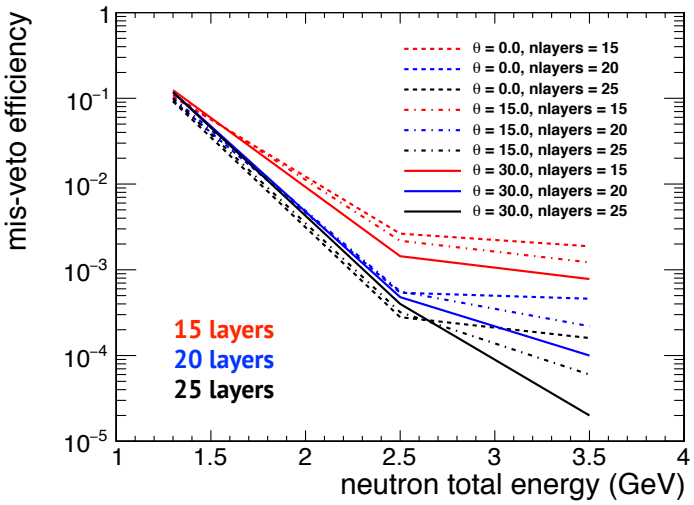

Figure 11. Number of MIP layers for a 2.5 GeV neutron produced with an incident angle of 0.0° at the front face of the calorimeter for a system of 15, 20, or 25 layers (left to right).

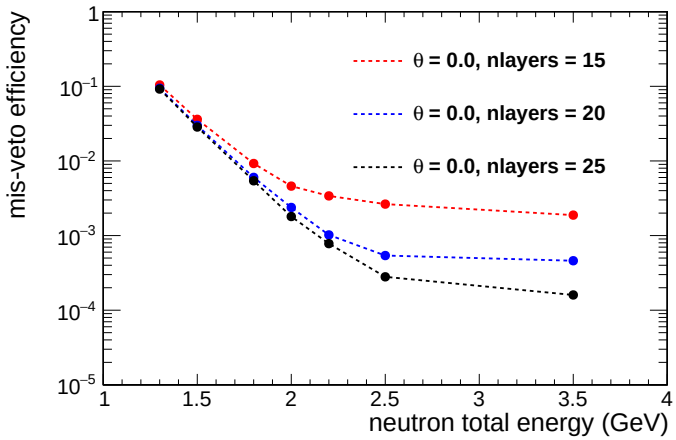

Figure 12. Number of MIP layers for a 2.5 GeV neutron produced with an incident angle of 0.0° at the front face of the calorimeter for a system of 15, 20, or 25 layers (left to right).

per $10^1 - 10^5$ for neutron kinetic energies ranging from 400 MeV to 2.5 GeV depending on number of layers in the system and incident angle. In the next Section, we study in more detail the veto capabilities of the entire calorimeter system, ECAL + HCAL, for rare photo-nuclear processes.

Figure 13. Performance of the primary physics trigger for LDMX. The effiency for signal electrons of differing energy and the trigger rate for all backgrounds induced by beam electrons are shown as a function of the trigger threshold in MIP units.

Table 1. Draft trigger menu for LDMX, showing the primary contributions to the trigger budget for a 40 MHz beam rate

Trigger	Prescale factor	Rate (Hz)
Physics Trigger	1	
E(ECAL) < 1.2 GeV		850
Background-Measurement Triggers		*100*
E(ECAL) > 3 GeV		25
E(ECAL) > 2 GeV		50
HCAL single MIP trigger		25
Detector-Monitoring Triggers		*50*
Beam-arrival (hodoscope)	4000000	10
Empty-detector (hodoscope veto)		10

Allocations are extremely rough at the moment!

5.6 Trigger Performance

As described above, the primary physics trigger is based on the total energy observed in the calorimeter, combined with a requirement of a single incoming electron observed in the trigger fiber hodoscope. Figure 13 shows the simulated performance of the primary physics trigger for signal and background.

Besides the primary physics trigger, the LDMX trigger system will also allow the selection of events for calibration, alignment, and background studies. The trigger will include input from the scintillator calorimeter to allow selection of events with hadrons or muons. Each event will be marked with the set of triggers which fired. An initial draft trigger menu is shown in Table 1.

1. What is the rate of muon production? We would expect to trigger these, yes?
2. What is the impact of cosmics on the HCAL trigger?

6 Budget and Schedule

6.1 DASEL (Editors: Philip Schuster, Gordan Krnjaic)

6.2 Tracking (Editors: Tim Nelson, Omar Moreno)

6.3 Forward ECal (Editors: Joe Incandela, Jeremy Mans)

6.4 Hadronic Veto (Editors: Jeremy Mans, Nhan Tran, Andrew Whitbeck)

6.5 Trigger (Editors: Jeremy Mans, Nhan Tran, Andrew Whitbeck)

6.6 DAQ (Editors: Jeremy Mans, Nhan Tran, Andrew Whitbeck)

6.7 Operations